



Citation for published version:

Margaris, P, Marles, D & Gursul, I 2008, 'Experiments on Jet/Vortex Interaction', Experiments in Fluids, vol. 44, no. 2, pp. 261-278. <https://doi.org/10.1007/s00348-007-0399-7>

DOI:

[10.1007/s00348-007-0399-7](https://doi.org/10.1007/s00348-007-0399-7)

Publication date:

2008

[Link to publication](#)

University of Bath

General rights

Copyright and moral rights for the publications made accessible in the public portal are retained by the authors and/or other copyright owners and it is a condition of accessing publications that users recognise and abide by the legal requirements associated with these rights.

Take down policy

If you believe that this document breaches copyright please contact us providing details, and we will remove access to the work immediately and investigate your claim.

Experiments on Jet/Vortex Interaction

P. Margaris, D. Marles and I. Gursul

An experimental study was performed to evaluate the effect of a cold jet on a single trailing vortex. Flow visualization and Particle Image Velocimetry (PIV) measurements were conducted in wind and water tunnels. The main parameters were the ratio of jet-to-vortex strength, the jet-to-vortex distance, the jet inclination angle and the Reynolds number. It was shown that the jet turbulence is wrapped around the vortex and ingested into it. This takes place faster with decreasing jet-to-vortex distance and increasing jet strength. Both time-averaged and instantaneous flow fields showed that the trailing vortex became diffused with its rotational velocity and vorticity levels reduced when the jet is located close to the vortex. The mechanism with which the jet interacts with the vortex is a combination of vortices shed by the jet and the turbulence. No noticeable differences were found within the Reynolds number range tested. The effect of jet on the vortex is delayed when the jet is blowing at an angle to the free stream and away from the vortex such as during take-off.

Nomenclature

A_j : jet nozzle exit area

b : wing span

c : airfoil chord length

d_j : jet nozzle diameter

h : jet-to-vortex distance

R : ratio of jet strength to vortex strength

Re : Reynolds number

U : cross-flow velocity magnitude

U_j : jet velocity

U_∞ : free stream velocity

U_0 : reference cross-flow velocity

P. Margaris

Department of Aerospace Engineering

University of Bristol, Bristol, BS8 1TR, UK

D. Marles, I. Gursul (corr-author)

Department of Mechanical Engineering

University of Bath, Bath, BA2 7AY, UK

email: I.A.Gursul@bath.ac.uk

u_{st} : standard deviation of cross-flow velocity

x : streamwise distance

y : spanwise distance

z : normal distance

ρ : density

Γ : circulation

α : angle of attack

ν : kinematic viscosity

α_j : jet incidence angle

ω : normalized vorticity

1 Introduction

Wing tip vortices have been the subject of research for many years due to problems associated with them. Induced drag (that can reach 40% of the total drag) and wake vortex hazard are the most well known; the latter is also the main reason behind the large number of studies in wing tip vortices in the last decade. The flow topology of the structure of the wake behind a transport aircraft in the near field is well understood (Spalart, 1998, Rossow, 1999). A vorticity sheet is shed behind the wing, which rolls-up into a number of concentrated vortices at a small distance downstream of the trailing edge. The behavior of the vorticity sheet depends on the flight phase. During cruise flight, the vorticity sheet rolls-up around the two vortices generated at the wing tips, and the near wake is dominated by a pair of counter-rotating vortices. When high lift devices are deployed (take-off and landing), the vorticity sheet rolls-up around more vorticity peaks, generated by the flap tips. Therefore, the wake behind each wing is composed of multiple co- and counter-rotating vortices. These vortices will eventually merge with the two tip vortices leading to a wake similar to the cruise flight.

In the attempt to manipulate the wake favorably, several means have been suggested. Some of the suggestions require the use of retrofitted devices whereas others attempt to achieve the target utilizing existing aircraft components. As such, the aircraft jet engines are a

very significant candidate, especially since the jet exits near the vorticity sheet generated by the flap-edge. However, in order to utilize them to manipulate the wake vortices, it is essential to have a good understanding of the effect of the jet on a single trailing vortex.

As in the case of the wake vortices, the co-flowing jets have been extensively studied and are well understood. The Kelvin-Helmholtz type instability has been found to be inherent in a jet profile and its growth rates have been studied for simple cases (Michalke and Hermann, 1982). However, the studies focused on the interaction between a jet and a vortex are fewer. Qualitatively, the interaction is separated in two phases (Miake-Lye *et al.*, 1993). In the first phase (jet regime) the jet mixes with the ambient air while the vorticity sheet rolls-up around the tip vortex. During this regime the interaction between the jet and the vortex is minimal (this has been the main assumption behind a number of simulations of the jet/vortex interaction as in Ferreira *et al.*, 2002, Paoli *et al.*, 2003, and Paoli *et al.*, 2004). The second phase (interaction regime) is dominated by the entrainment of the jet into the vortex.

Using a delta wing as vortex generator and with a jet blowing along the centerline, Wang *et al.* (2000) showed that the effect of the jet on the trajectory of the vortices is minimal whereas the jet was significantly influenced by the vortices. The jet lost its axisymmetric shape and was compressed vertically and elongated horizontally. In a further study (Wang and Zaman, 2002), it was shown that the vortex induced flow results in the generation of vortices around the jet. The strength of these vortices is significant and leads to the deformation (stretching) of the jet. Secondary vortices have also been observed (Ferreira *et al.*, 2002, Paoli *et al.*, 2003, and Paoli *et al.*, 2004) forming at the periphery of the vortex due to the effect of the axial velocity of the jet, when the initial separation between jet and vortex is large. These structures lose coherence further downstream without penetrating into the core (Ferreira *et al.*, 2002). On the other hand, when the jet is blowing very near the core, similar to a q-vortex (Batchelor, 1964) and the jet-to-vortex velocity ratio is high, the tip vortex will diffuse rapidly but maintain its total circulation (Paoli *et al.*, 2003).

In a comparative numerical and experimental study (Huppertz *et al.*, 2004), a number of jet-to-vortex distances were examined for two jet velocities. The results showed good qualitative agreement between the simulation and the experiment. The jet was shown to have a small impact in the tangential velocity of the vortex for all jet-to-vortex distances and jet velocities whereas the distance between the jet and the vortex affected the axial vortex velocity significantly. Many studies have focused on the effect of the vortex on the jet, either for acoustic reasons (Seiner *et al.*, 1997) or for studying environmental issues connected with the mixing of the pollutants produced by the jet engine in the tip vortex (Jacquin and Garnier, 1996, Garnier *et al.*, 1997, Brunet *et al.*, 1999, Paoli *et al.*, 2003 and Paoli *et al.*, 2004). Both experiments and simulations (Seiner *et al.*, 1997) verified that the initially axisymmetric jet was distorted and evolved into a non-circular structure, which was assumed to lead to a non-symmetric sound radiation. Experiments (Jacquin and Garnier, 1996) also showed that even in the near wake, where the jet possesses significant velocity, part of it is entrained into the vortex.

The purpose of the present study is to conduct an extensive parametric study on the effect of a co-flowing engine jet on a wake vortex. Although most researchers have focused on the effect on the jet, accepting that the effect on the vortex is minimal (unless the jet-to-vortex distance is significantly small), an extensive experimental study is required to quantify the effect and to understand the jet/vortex interaction. In addition, the use of a PIV system will provide information about the instantaneous flow fields; information both valuable (due to the unsteady nature of the flow) and also not possible to obtain with point measurements used in previous studies. The current study will focus on four main parameters: the jet-to-vortex distance, their relative strengths, the jet-to-freestream angle and the Reynolds number in an attempt to provide a sound database for future research efforts.

2 Experimental setup

In order to gain a better understanding of the phenomenon, several experiments were conducted in different facilities. Experiments were carried out in the water and wind tunnel facilities of the Department of Mechanical Engineering at the University of Bath. The water tunnel was used for both qualitative and quantitative measurements (flow visualization and PIV measurements respectively) whereas the wind tunnel was used for quantitative measurements at higher Reynolds numbers.

The water tunnel is an Eidetics Model 1520 free surface tunnel with a 0.381 m x 0.508 m x 1.524 m test section. The maximum speed of the water tunnel is 0.45 m/s. The tunnel has four viewing windows, three surrounding the test section and one downstream allowing axial viewing. The tunnel also incorporates a dye system with six available dye tubes to enable flow visualization with different colors.

The model used in this facility consisted of a rectangular wing with a 5% cambered section and constant 2% thickness. The wing was mounted upside down from the top of the test section about 150 mm downstream of the end of the contraction section (see Fig. 1). The semispan of the wing (part in the water) was 230 mm and the chord was 40 mm, giving an aspect ratio of 11.5 (based on the full span). The jet was simulated using a nozzle supplied with mains water through the jet support. The jet support was secured next to the wing and was streamlined and L-shaped so that the jet support / wing interference would be kept to a minimum. The nozzle had an internal diameter of 6 mm, a wall thickness of 0.5 mm and its last section (the part extending from the support) was straight and had a length of 40 mm. A schematic of the setup is shown in Fig. 1.

The wind tunnel used was the 7' x 5' closed circuit tunnel. The high speed test section of this tunnel measures 2.134 m x 1.524 m x 2.700 m and the maximum velocity is 45 m/s. The model used in this facility was a rectangular wing with a NACA 0012 airfoil section, a square tip, a semispan of 500 mm and a chord of 100 mm (aspect ratio 10 when based on full span).

The wing was mounted vertically on the floor of the tunnel with its leading edge 150 mm from the beginning of the test section (see Fig. 2). The jet was simulated using a nozzle which was supplied with air through its support. The jet support was located inside the test section and was streamlined throughout its length. In order to minimize the interference of the support to the measured flow the support had an inversed L shape so that the part extending parallel to the wing was positioned as far from the wing as possible. The diameter of the jet was 15 mm and the wall thickness throughout the final section of the nozzle 1 mm. The final section was straight and had a length of 60 mm. A honeycomb positioned before the final section was used for flow conditioning in the nozzle. A schematic of the experimental setup is shown in Fig. 2.

Flow visualization was conducted in the water tunnel, using fluorescent dye and an Argon-Ion laser. Green (Rhodamine 6G) and red (Rhodamine B500%) dyes were used to distinguish between the vortex and jet flows respectively. The jet dye was fed to the jet at the base of the support and by the time it had reached the jet exit it had mixed with the main jet flow. The wing dye was released from the midpoint of the wing tip. The laser used was a water cooled Coherent Innova70 4 Watt Argon-Ion continuous emission system emitting a laser beam at a wavelength of 515 nm which, by passing through a cylindrical and a spherical lens, illuminated a cross-flow plane. As a result the dye fluoresced at this plane making the flow structure visible to a digital video camera recording at 25 frames per second. The camera was positioned outside the test section looking through the rear axial viewing window. Still images were then extracted from the video for analysis. Time-averaged fields were produced by superimposing 10 instantaneous images (the images were made partly transparent).

Quantitative measurements were obtained using a Digital Particle Image Velocimetry (DPIV) system. It was a 2-D TSI Powerview system, which incorporates a 120 mJ dual Nd:YAG laser system and a CCD camera. A cylindrical lens was used to generate the laser sheet. The laser was positioned on a traverse system enabling it to move to the specified

streamwise station. The camera, which has a capability of recording images of 2048 x 2048 pixels at 8-bit grayscale at a maximum rate of 3.75 pairs/second, was positioned behind the wing at a position far enough to minimize its effect on the flow field in the wind tunnel experiments. For the water tunnel experiments, that was not a problem since the camera was not in the flow but was able to see the wing through the axial viewing window of the tunnel. Since the wind tunnel did not have this facility, the camera was positioned at the end of the test section. Seeding in the wind tunnel was implemented using a TSI six-jet atomizer generating oil particles of 1 μm diameter. In the water tunnel the flow was seeded using commercially available neutrally buoyant hollow glass particles of mean diameter of 8 – 12 μm .

Sets of 100 to 200 pairs of images were recorded for each experiment at a rate of 3.75 Hz. For the analysis of these images, cross-correlation was used by implementing the Hart algorithm with an interrogation window of 32 x 32 pixels and 50% overlapping. Some experiments required a 16 x 16 pixels interrogation window to achieve the required spatial resolution which was equivalent to about 1% of the chord. The time-averaged results presented were produced by averaging the instantaneous flow fields for each case. The instantaneous fields were also analyzed independently. The estimated uncertainty for velocity measurements is 2%.

3 Results

A large number of cases were tested for different vortex strengths, jet to free stream velocity ratios and jet-to-vortex distances. The first two parameters are combined by using the R parameter, which is defined as:

$$R = \frac{\rho_j U_j (U_j - U_\infty) A_j}{\rho \Gamma^2} \quad (1)$$

where ρ_j is the jet density, U_j is the average jet velocity, U_∞ is the free stream velocity, A_j is the jet area, ρ is the density of the free stream, and Γ is the circulation strength of the vortex.

The vortex strength (circulation) was controlled by the angle of attack of the vortex generating wing. Most experiments were conducted at an angle of attack of 10° although some experiments were carried out for $\alpha = 5^\circ$, which resulted in weaker vortices and higher R values. The jet strength was controlled by the jet to free stream velocity ratio, which was in the range from 1.88 to 4.03. This range compares well with the suggested values (de Bruin, 2005), especially for the take-off and approach phases.

The parameter space covered by the experiments can be seen in Fig. 3 as well as the R values from previous experiments found in the literature and the estimated R values for two airplanes in cruise (C) and take-off (T) configurations. The estimated airplane R values were calculated using the engine thrust data and estimated vortex strength. For the cruise condition the vortex circulation was calculated assuming an elliptical lift distribution and both thrust and engine exhaust diameter were found from the engine manufacturer's data. The estimated values for cruise condition is $R = O(1)$. In the case of take off condition, there are larger uncertainties in the estimated value of the parameter R , therefore resultant values are significantly higher than realistic R values. The jet thrust used was the sea level static thrust (manufacturer's data) which is higher than the actual thrust during take-off. The flap vortex was chosen instead of the tip vortex since it is closer to the jet. Note that, typically, flap vortices are stronger than the tip vortices during landing, but weaker during take off. As a typical value, the flap vortex circulation was taken to be about 1/3 of the total bound circulation (which was again calculated assuming elliptical lift distribution and take-off speed). Hence the two data points marked as T (take off) for airplanes represent the upper bound. More realistic values for take off might be about 50% of the upper bound, especially because the thrust is overestimated.

The distance h/d_j plotted in the graph is not the actual jet-to-vortex distance but the distance measured from the centre of the jet to the trailing edge point of the wingtip as shown in Fig. 4. Figure 4 also shows the two traversing directions used during preliminary experiments. The difference in the results between horizontal and vertical traversing was insignificant (Margaris *et al.*, 2006), therefore vertical traversing was chosen for the main experiments. The nozzle exit is located at the same streamwise location as the trailing edge of the rectangular wing and its spanwise position is at the wing tip, unless otherwise indicated. This is not representative of an aircraft configuration; nevertheless, the simplified wing used in the experiments was treated as a vortex generator and not a typical aircraft wing.

One more important parameter was the Reynolds number of the flow. Table 1 shows a collection of the Reynolds numbers for all the experiments conducted at $\alpha = 10^\circ$ in both facilities. The three Reynolds numbers presented are:

$$\text{Re}_c = \frac{U_\infty c}{\nu} = \text{Reynolds number based on the chord length of airfoil}$$

$$\text{Re}_\Gamma = \frac{\Gamma}{\nu} = \text{Reynolds number based on the circulation of the vortex}$$

$$\text{Re}_{d_j} = \frac{U_j d_j}{\nu} = \text{Reynolds number of the jet.}$$

The circulation Reynolds number was calculated using the circulation derived from the time-averaged velocity field of the reference case (no nozzle in the flow) for the first downstream station measured in each facility, which is $x/b = 0.35$ for water tunnel experiments and $x/b = 0.40$ for wind tunnel experiments. The uncertainty in the circulation calculation is less than 2%.

Another parameter investigated was the jet incidence angle, which might be important during take-off and landing. Typical values suggested (Jupp, 2004, private communication) are $\alpha_j \approx 13^\circ$ for take off and $\alpha_j \approx 6^\circ$ for landing. Hence, the parameter values used in the current experiments were $\alpha_j = 5^\circ, 10^\circ$ and 15° .

Table 1. The Reynolds number range of the experiments.

	Re_c	Re_r	Re_{dj}
Water tunnel	10000	5500	3200
			4500
			6400
Wind tunnel	70000	14000	19300
			27200
			38600
	140000	33000	38600
			54500

The first step of the experimental campaign was to get a qualitative understanding of the jet effect on the wing tip vortex. In order to achieve that, a series of flow visualization experiments was conducted in the water tunnel facility. Fig. 5 shows two images obtained with the digital video camera. These images represent instantaneous flow fields. The first image shows the flow field at 0.35 spans downstream of the trailing edge of the wing. The jet-to-tip distance is 6.7 jet diameters ($h/d_j = 6.7$) and the jet velocity is 2.01 times the free stream velocity ($U_j/U_\infty = 2.01$, $R = 0.13$). The white horizontal line represents the projection of the trailing edge on the illumination plane whereas the circle is the projection of the jet nozzle. It can be seen that at this downstream position there is still no visible interaction between the jet and the vortex. However, it is seen that the jet has spread out as expected. In the second image, taken at 1.75 spans downstream of the trailing edge, the jet is seen to have been elongated and rotated due to the cross-flow velocity field around the vortex. The one end of the jet has been wrapped around the vortex. At this streamwise position the effect of the jet on the vortex appears to be significant.

Figure 6 shows two instantaneous fields taken at $x/b = 1.75$ and at the same R value as for Fig. 5 but with the initial jet-to-tip distance being smaller ($h/d_j = 4$). By comparing Figs 6a and 5b it becomes obvious that when the jet is closer to the vortex it gets wrapped around it faster and thus affects it more. Almost all of the jet structure is seen around the vortex core at 1.75 spans downstream of the trailing edge for $h/d_j = 4$. Fig. 6b shows an instantaneous image

from the same case but only the jet is visualized. This image illustrates that the jet gets wrapped around the vortex and also penetrates into the core.

Figure 7 shows the streamwise development of the time-averaged flow. Time-averaging of the flow visualization images has been achieved by introducing a degree of transparency in each image and then superimposing all of them. As in the previous figures the jet velocity is almost twice the free stream velocity ($U_j/U_\infty = 2.01$, $R = 0.13$). The jet-to-tip distance is $h/d_j = 6.7$; Figs 7a and 7e are time-averaged images of the same cases as seen in Figs 5a and 5b respectively. It is clear from this set of images that the jet spreads in the radial direction but also rotates around the vortex. The end of the jet structure that is closer to the vortex rolls around the vortex core.

The jet turbulence is believed to be the main mechanism with which the jet interacts with the tip vortex in the near wake. This can be made clearer by examining the PIV data. The comparison between Figs 5b and 6a showed that the initial jet-to-tip distance is an important parameter; the closer the jet to the vortex the faster it gets wrapped around and interacts with it. Figure 8 shows the standard deviation of the cross-flow velocity for three different cases. All these cases were in the water tunnel at $x/b = 0.35$ and $U_j/U_\infty = 2.85$ ($R = 0.34$). The low frame rate of the PIV cannot allow for the actual turbulence to be measured but the standard deviation of the cross-flow velocity is a quite good qualitative measure. In the graphs the effect of the wing wake (as well as the jet support) is visible but, more importantly, the levels of turbulence in the jet clearly dominate the field. This shows the importance of the turbulence of the jet. By moving the jet closer to the vortex, this turbulence gets ingested in the vortex core faster and also increases the overall core unsteadiness.

Figure 9 shows the streamwise development of the standard deviation of the cross-flow velocity for one of the cases of Fig. 8 ($h/d_j = 4$, $U_j/U_\infty = 2.85$, $R = 0.34$). The jet turbulence gets wrapped around the vortex core exactly as it has been observed in the flow visualization images. In fact, by comparing the flow visualization images with the standard deviation

contour plots, it can be seen that the turbulence of the jet can be used to visualize the jet. Moreover, it is observed that the turbulence levels of both the jet and the vortex decrease with downstream distance. However, the decay of turbulence is much faster for the jet. This stresses the importance of the initial jet-to-vortex distance. If the distance is large enough, the jet turbulence is expected to have decayed significantly before interacting with the vortex, thus leading to a minimal effect. It is not clear whether the persistence of unsteadiness in the core is due to the ingestion of jet turbulence only. Some part of the cross-flow velocity fluctuations is probably due to the vortex wandering phenomenon. One last observation from this figure is that the turbulence levels due to the wing wake decay fast so their effect should be negligible about one span downstream of the trailing edge. Hence, this suggests that the wing wake turbulence might not be as important as the jet turbulence when the jet / vortex interaction is considered.

Although the standard deviation plots help to visualize the jet, the best way to identify the effect it has on the vortex is by examining the cross-flow velocity and vorticity fields. Figs 10 and 11 show the time-averaged cross-flow velocity magnitude and vorticity distributions respectively, as obtained from experiments in the water tunnel at $x/b = 1.05$ and for $h/d_j = 4$ for three different R parameters ($U_j/U_\infty = 2.01$, $U_j/U_\infty = 2.85$, $U_j/U_\infty = 4.03$) plus one “control” case ($U_j/U_\infty = 0$). This is not the standard reference case (when there is no nozzle in tunnel) but is the case used to check the effect of the jet nozzle on the wake vortex. The jet nozzle is in position but the jet velocity is zero. The R parameter would be zero if $U_j = 0$ was used but that would not be representative since the jet nozzle creates a wake when it is not blowing. It can be seen that by increasing the blowing of the jet (increasing R) the effect of the jet on the vortex is more pronounced.

The introduction of blowing proves to affect the vortex by reducing the cross-flow velocity magnitude levels (Fig. 10b), and an increase in the jet exit velocity (increase in the R parameter) results in an even more diffused vortex (Figs 10c and 10d). The same conclusion

can be derived from Figs 11b to 11d; the vorticity levels in the core of the vortex are reduced with increasing R . It should be noted that (due to the deflection of the jet by the vortex) the jet can be seen in the cross-flow velocity magnitude plots as increased cross-flow velocity levels at the lower right corner of each plot whereas no vorticity (comparable to the vorticity of the core) is observed in the same area. A comparison with the standard deviation plots easily demonstrates that the turbulence plots are the best way to visualize the jet in a cross-flow plane.

However, at an upstream location ($x/b = 0.35$), vortical structures shed from the jet were identified. Figure 12a shows the time-averaged vorticity field for $U_j/U_\infty = 2.01$ and $h/d_j = 6.7$ (same condition as in flow visualization shown in Fig. 7a). A pair of counter-rotating vortical structures is seen near the jet, apparently due to the cross-flow induced by the vortex. The vorticity levels of these structures are quite low compared to the vorticity levels in the vortex core. Examining the instantaneous fields, however, shows that the vortical structures due to the jet can become comparable to the tip vortex. Figure 12b shows the vorticity distribution of an instantaneous field for $U_j/U_\infty = 4.03$ and $h/d_j = 4$. The jet vorticity is believed to originate from the counter-rotating vortex pair shed from the jet due to the rotational velocity of the vortex (similar to a jet in cross-flow) and the jet turbulence, which contains substantial negative vorticity when the R value is high and the jet close to the vortex. Although the jet vorticity is barely visible further downstream it has contributed in the development of the near wake and the reduction of vorticity levels in the vortex core.

It should be noted that the time-averaged data should be viewed with caution with regard to the observation of diffused vortices with jet blowing. Vortex wandering could also increase the vortex core size, leading to the apparent diffused structure. Figure 13 compares the vortex center position of the time-averaged field to the vortex center of the instantaneous flow fields for a number of cases tested. The time-averaged vortex center is shown with black symbols whereas the instantaneous vortex centers are shown with gray symbols. The error bars present

the standard deviation of the core movement in each direction. Using the standard deviation to calculate the amplitude of wandering, this quantity is estimated at 29% of the core radius for the reference case (Fig. 13a). This value compares very well with the 30% reported by Devenport *et al.* (1996). The introduction of the nozzle increases the vortex wandering by a small amount (amplitude reaches 35% of the core radius) as seen in Fig. 13b. However, the jet effect is much more significant. Even for the lowest R value (Fig. 13c) the amount of wandering has increased significantly over the previous two cases (45% of the time-averaged core radius). Increasing the jet momentum leads to even more pronounced wandering motion, as can be seen in Figs 13d and 13e, with the wandering amplitude reaching 93% and 110% of the time-averaged vortex core radius respectively.

The above results show that the time-averaged fields are heavily influenced by the vortex wandering effect. Nevertheless, the examination of the time-averaged fields can be supported by the analysis of the instantaneous fields. The advantage of using the instantaneous fields is that they can reveal structures that can get lost in the averaged field. In a study where turbulence is of great importance the instantaneous fields should not be overlooked. Figures 14 and 15 present a set of instantaneous cross-flow velocity and vorticity plots for two experimental cases ($h/d_j = 2.7$ in Fig. 14 and $h/d_j = 4$ in Fig. 15). In both cases the downstream location is at $x/b = 1.05$ and the velocity ratio is $U_j/U_\infty = 2.85$. The relatively high R value results in more pronounced effects that are easier to identify visually.

The instantaneous fields shown are a representative selection from the 100 fields collected for each case. The field shown in Figs 14a and 14b is from the no blowing reference case (nozzle in the tunnel but $U_j = 0$). No other fields from this experiment are shown because the differences between them are very small (mainly the position of the vortex due to wandering). When the jet is not blowing the tip vortex essentially remains coherent. When blowing is applied ($U_j/U_\infty = 2.85$, $R = 0.34$) the flow changes significantly. The vortex is no longer coherent and the cross-flow velocity magnitude levels are decreased. A region of

rather high velocities appears in some instantaneous fields, outboard of the tip (Fig. 14c) whereas it is not evident in others (Fig. 14e). This velocity excess can only be attributed to the jet. These large variations of cross-flow velocity in that region are consistent with increased turbulence as it is already seen in the standard deviation plots. The vorticity fields do not show a coherent vortex but multiple peaks in the area of the tip vortex as well as increased vorticity levels outboard of the wing.

Moving the jet further away from the vortex (Fig. 15, $h/d_j = 4$) reduces the effect of the jet on the vortex. The no blowing instantaneous field (Figs 15a and 15b; again only one representative field is shown) reveals a slightly more coherent vortex. This is attributed to the increased distance between the wing and the jet nozzle leading to decreased interaction. When the jet is blowing ($U_j/U_\infty = 2.85$, $R = 0.34$), the vortex appears diffused and broken down as in the previous case but at a smaller level. The cross-flow velocity and vorticity levels around the vortex are higher than the ones seen in Fig. 14. However, multiple vorticity peaks are still visible. The higher velocities seen outboard of the wing in the previous case are also seen in some of the instantaneous fields but they are clearly more prominent and also appear in the lower right part of the field (Fig. 15c). Increased vorticity is also seen in these regions (Fig. 15d). This is consistent with the conclusions derived so far. These velocities have been attributed to the jet and the highest jet turbulence levels are expected to be where these velocities are observed (in the instantaneous fields). This suggests that a significant part of the jet still remains in the lower right corner of the image whereas in Fig. 14 most of the jet has been seen to move closer to the vortex. For the same R value and the same downstream distance a smaller part of the jet has moved closer to the vortex for the higher jet-to-tip distance; exactly as seen in the flow visualization (compare Figs 5b and 6a) and the standard deviation plots (Fig. 8). Clearly, the increased jet-to-tip distance has led to a reduced interaction between the jet and the vortex at this downstream location.

The PIV results shown so far are representative of a large amount of data. By analyzing the PIV data, a summary of flow properties calculated has been created. Fig. 16 shows the maximum cross-flow velocity magnitude around the core of the vortex as a function of the R parameter and the jet-to-tip distance (h/d_j), for the data obtained at 1.4 spans downstream of the trailing edge ($Re_\Gamma = 5500$). The values are normalized by the equivalent time-averaged value (U_0) for the reference case (no nozzle in the tunnel) at $x/b = 0.35$ (the first station measured). This velocity was found to be 36% of the free stream velocity. The horizontal lines show the cross-flow velocity magnitude of the reference case at $x/b = 1.4$, the circles show the cross-flow velocity magnitude when the jet nozzle is in the flow but not blowing and the other symbols refer to the three blowing velocities used. The solid lines and filled symbols refer to the data obtained from the analysis of the time-averaged fields whereas the dashed lines and hollow symbols show the mean value obtained from the analysis of the 100 instantaneous fields for each experiment.

This graph illustrates the importance of the $U_j = 0$ experiments. It is clear that the nozzle interference is significant for the two smallest h/d_j distances, whereas it becomes negligible for distances larger than $h/d_j = 4$. There are two different mechanisms by which this interference plays a role. Firstly, when the nozzle is very close to the wing, the vortex formation is affected. Secondly, the wake flow behind the nozzle is the source of turbulence that gets ingested into the vortex. Although the effect of jet blowing appears to be very large for the smallest h/d_j case (when compared to the reference case) the actual effect is partly due to the interference of the nozzle itself. Only cases with $h/d_j > 4$ can be considered to be representative of the vortex / jet interaction for this downstream location. Further downstream the jet nozzle interference is expected to be present for these cases as well.

It can be seen from the graph that the effect of the jet is more pronounced when the jet is closer to the tip (which means closer to the vortex) and when the R parameter is increased (higher U_j/U_∞). The effect appears to reach an asymptotic maximum for the highest R value

and for the smallest h/d_j distance. This is attributed to the already much diffused vortex (due to nozzle interference as well). On the other hand, the jet effect appears to be minimal when the initial distance is large even for high R values. Based on the previous discussion on the decay of the jet turbulence, it can be assumed that there is a limit in the initial jet-to-vortex distance, above which the jet has practically no effect on the vortex. However, there is not enough information to suggest that this limit is within the distances presented in the graph.

Finally, the direct comparison of the time-averaged and instantaneous results clearly shows that both sets follow the same trend but the instantaneous values are larger than the time-averaged. This is because of the vortex wandering which results in a smeared time-averaged field. The instantaneous value is 19% higher than the time averaged for the reference case, which compares well with the 15% reported by Devenport *et al.* (1996). The instantaneous results are useful for complementing the time-averaged data.

For a more detailed study of the results, the wind tunnel data are used because of the higher Reynolds number ($Re_\Gamma = 14000$). Figure 17 shows the mean instantaneous maximum cross-flow velocity magnitude for the four x/b stations measured in the large wind tunnel. The horizontal dashed line represents the reference (no nozzle) case. As for the previous graph, all the values have been normalized using the time-averaged cross-flow velocity magnitude of the reference case at the first downstream station (found to be 30% of the free stream velocity, which compares well with that reported by Devenport *et al.* (1996)). It can be seen that at the first downstream location the only effect is for high blowing (large R values) and small h/d_j distance. For the minimum h/d_j distance, the effect of the jet nozzle is obvious at only 40% of the span downstream of the trailing edge (Fig. 17a). By moving downstream (Figs 17b to 17d), the effect of the blowing jet is larger for the low h/d_j cases. The interference of the nozzle is also seen to increase. Moreover, the jet appears to affect the vortex even for larger initial separation distances. In summary, it is clear that the introduction

of the jet results in a diffused vortex with lower maximum cross-flow velocity magnitude in the core.

The above set of graphs presents the effect of the jet-to-tip distance and of the R parameter for a given Reynolds number ($Re_\Gamma = 14000$). In order to study the Reynolds number effect, experiments were conducted in the wind tunnel at a higher free stream velocity and a circulation Reynolds number of $Re_\Gamma = 33000$. Figure 18 presents the results of these experiments at $x/b = 1.2$. The two properties presented are the maximum cross-flow velocity magnitude obtained from the time-averaged flow and the instantaneous flow (for the latter, the mean value from 100 images is presented). The values have been normalized by the equivalent time-averaged value for the reference case at $x/b = 0.4$ (as for the lower Reynolds number experiments). This streamwise location of the measurement plane has been chosen because it is far enough from the trailing edge so that the effect of the jet is more likely to be visible. Only two R parameters were investigated. Although the U_j/U_∞ ratio is the same as for the lower Reynolds number experiments, the actual R values differ slightly. That is due to different normalized circulation values for the reference case vortex; a Reynolds number effect on the vortex formation at these low Reynolds numbers around airfoils.

The graphs present the same trend as the graphs in Figs 16 and 17 and do not show a great sensitivity to the Reynolds number. The only significant difference is the very low cross-flow velocity magnitude observed in Fig. 18b for $h/d_j = 1.3$, but at this small jet-to-tip distance and for high blowing the vortex is too diffused and thus the results are more sensitive. It should be noted however that the high Reynolds number results show a better consistency especially for the larger h/d_j distances (clearly no jet effect).

One more parameter that has been examined is the angle between the free stream velocity and the jet velocity. The definition of this angle is shown in Fig. 19. Experiments were conducted in the wind tunnel at the low Reynolds number ($Re_\Gamma = 14000$) at 1.2 spans downstream of the trailing edge. Both positive and negative jet inclination angles were tested.

Although only positive angles are actually found in aircraft applications, the use of negative angles increased our understanding of the phenomenon. Figure 20 presents the results from the analysis of these experiments. The property shown is the mean value of the maximum cross-flow velocity magnitude around the core of the instantaneous fields. The jet-to-tip distance is fixed at $h/d_j = 4$. This distance was chosen because it offers insignificant interference from the jet nozzle/support (at $x/b = 1.2$) as well as easily measurable effect of jet blowing.

The slight reduction in the maximum cross-flow velocity magnitude seen for increasing positive jet inclination angles is attributed to increased interaction from the support. Although the jet exit is still located 4 jet diameters from the wingtip, the part of the nozzle upstream of this has moved closer to the wing to achieve the desired angle. This is verified by the trend shown by the $U_j/U_\infty = 0$ points on the graph for positive jet inclination angles. The effect of blowing for positive angles is seen to be minimal at this downstream position. Further downstream the jet is expected to interfere with the vortex but having lost a larger part of its energy and turbulence it would probably produce a smaller or even negligible effect.

By moving to negative jet inclination angles the jet nozzle interference is significantly reduced since the nozzle has now moved further from the wing. The effect of blowing is much larger than in the case of $\alpha_j = 0^\circ$, especially for high R values. In these experiments the jet is pointing towards the vortex. As a result, more of the jet turbulence will be ingested in the vortex core and faster (closer to the trailing edge). The plateau seen for $\alpha_j = -10^\circ$ and $\alpha_j = -15^\circ$ could suggest an optimum jet inclination angle. Further experiments on this aspect could be useful for flow control purposes.

4 Conclusions

The purpose of this experimental campaign was to perform a parametric study on the effect of a cold jet on a single vortex. Large numbers of experiments were conducted in two

facilities (water and wind tunnel) in order to obtain a better understanding of the phenomenon. The main parameters that were examined were the R parameter (ratio of jet strength to vortex strength), the initial distance between the jet and the vortex, the jet inclination angle, the Reynolds number and the downstream distance from the trailing edge. It was shown that the jet turbulence is wrapped around and ingested into the vortex with increasing streamwise distance. This turbulence ingestion becomes more effective with decreasing jet-to-vortex distance and increasing jet strength.

Both time-averaged and instantaneous flow fields showed that the effect of the jet on the vortex can be quite significant. The trailing vortex became diffused with its rotational velocity reduced and its vorticity spread over a larger area. This result was achieved faster (closer to the trailing edge of the wing) for higher R parameters (stronger jet) and lower initial jet-to-vortex distances. The mechanism through which the jet interacts with the vortex is a combination of the vortices shed by the jet (because of the vortex induced velocity) and the turbulence. As a result, the faster the jet turbulence wraps around the vortex core the faster the vortex will be influenced. Moreover, the faster the jet turbulence interacts with the vortex, the more effective it will be since the turbulence levels will still be high. On the other hand, if the jet/vortex interaction is delayed, the jet turbulence levels will be so low as to not affect the vortex in any way. No noticeable differences were found within the Reynolds number range tested.

The effect of jet on the vortex is delayed when the jet is blowing at an angle to the free stream and away from the vortex (such as during take-off). On the other hand, if the angle is such that the jet is blowing towards the vortex, the latter is diffused a lot more and faster. Although this does not represent any realistic flight part, it could be used as a basis for flow control applications.

The use of a PIV system was proven to provide a significant advantage over point measurement techniques, since it provided information on the unsteady nature of the flow.

The analysis of the instantaneous fields removed the vortex wandering effect which affected the time-averaged measurements. The instantaneous fields also revealed vortical structures in the jet due to the trailing vortex; structures not visible in the time-averaged fields.

The results suggest that the engine jets might have favorable effects on wing vortices, causing faster diffusion. This applies mainly to flap-edge vortices, due to their small distance from the engine jet. During take-off high thrust is needed, but typically the flap-edge vortex is weaker than the tip vortex. Hence the favorable effect of the jet is only for the already weak vortex. It remains to be seen how the jet affects vortex merging in the near-wake. In addition, the effects further downstream should be investigated as the current results are limited to the near-wake region.

Acknowledgements

This work has been performed with the support from EC 6th Framework Programme Project "FAR-Wake".

References

- Batchelor GK (1964) Axial Flow in Trailing Line Vortices. *J Fluid Mech* 20:645-658
- Brunet S, Garnier F, Jacquin L (1999) Numerical/Experimental Simulation of Exhaust Jet Mixing in Wake Vortex. In: 30th AIAA Fluid Dynamics Conference, Norfolk, Virginia, USA (AIAA 99-3418)
- Devenport WJ, Rife MC, Liapis SI, Follin GJ (1996) The structure and development of a wing-tip vortex. *J Fluid Mech* 312:67-106
- de Bruin AC (2005) Estimation of Exhaust Velocities and Temperatures for Various Operation Phases of a Modern High By-Pass Turbofan. FAR-Wake Report D 2.1.1-1b, NLR
- Ferreira Gago C, Brunet S, Garnier F (2002) Numerical Investigation of Turbulent Mixing in a Jet/Wake Vortex Interaction. *AIAA J* 40:276-284
- Garnier F, Brunet S, Jacquin L (1997) Modelling Exhaust Plume Mixing in the Near Field of an Aircraft. *Ann Geophys* 15:1468-1477
- Huppertz G, Fares E, Abstiens R, Shroder W (2004) Investigation of Engine Jet/Wing-Tip Vortex Interference. *Aero Sci Tech* 8:175-183

- Jacquín L, Garnier F (1996) On the Dynamics of Engine Jets Behind a Transport Aircraft. AGARD-CP-584 37
- Margaris P, Marles D, Gursul I (2006) Experiments on Single Vortex/Jet Interaction. FAR-Wake Report TR 2.1.1-1, University of Bath
- Miake-Lye RC, Brown RC, Kolb CE (1993) Plume and wake dynamics, mixing and chemistry behind a high speed civil transport aircraft. *J Aircraft* 30:467-479
- Michalke A, Hermann G (1982) On the Inviscid Instability of a Circular Jet with External Flow. *J Fluid Mech* 114:343-359
- Paoli R, Laporte F, Cuenot B, Poinso T (2003) Dynamics and Mixing in Jet/Vortex Interactions. *Phys Fluid* 15:1843-1860
- Paoli R, Helie J, Poinso T (2004) Contrail Formation in Aircraft Wakes. *J Fluid Mech* 502:361-373
- Rossow VJ (1999) Lift-Generated Vortex Wakes of Subsonic Transport Aircraft. *Progr Aero Sci* 35:507-660
- Seiner JM, Ponton MK, Jansen BJ, Dash SM, Kenakowski DC (1997) Installation Effects on High Speed Plume Evolution. ASME FEDSM97-3227
- Spalart PW (1998) Airplane Trailing Vortices. *Annu Rev Fluid Mech* 30:107-138
- Wang FY, Proot MJ, Charbonnier J-M, Sforza PM (2000) Near-Field Interaction of a Jet with Leading-Edge Vortices. *J Aircraft* 37:779-785
- Wang FY, Zaman KBMQ (2002) Aerodynamics of a Jet in the Vortex Wake of a Wing. *AIAA J* 40:401-407

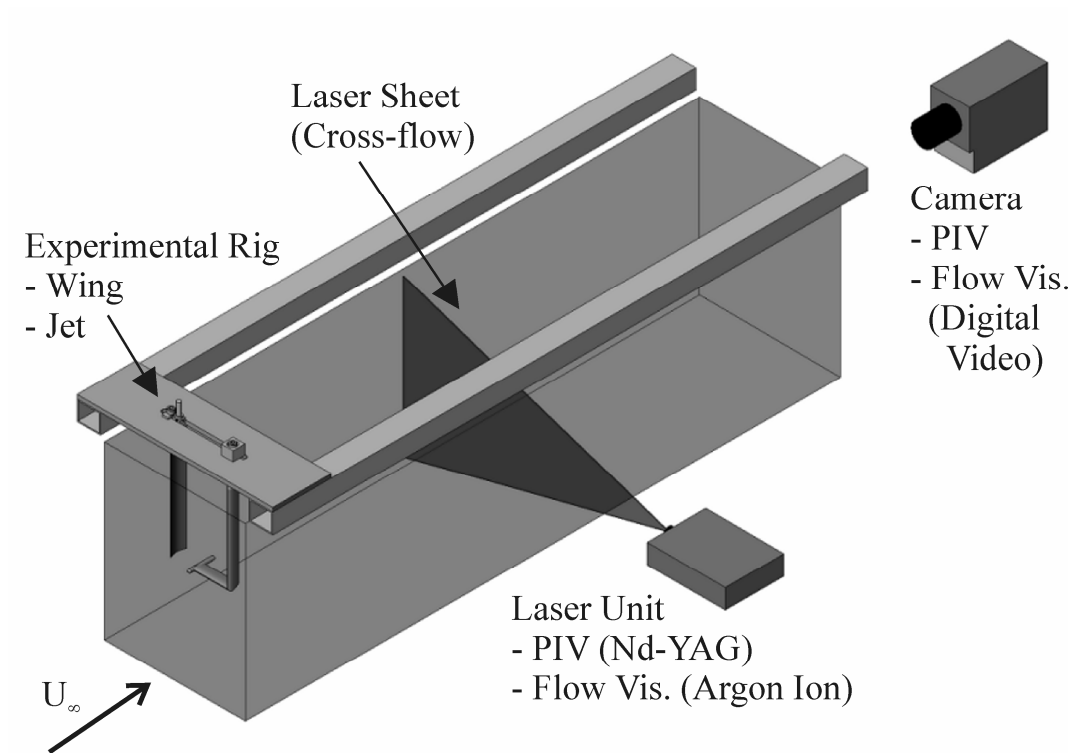


Figure 1. Experimental setup in water tunnel.

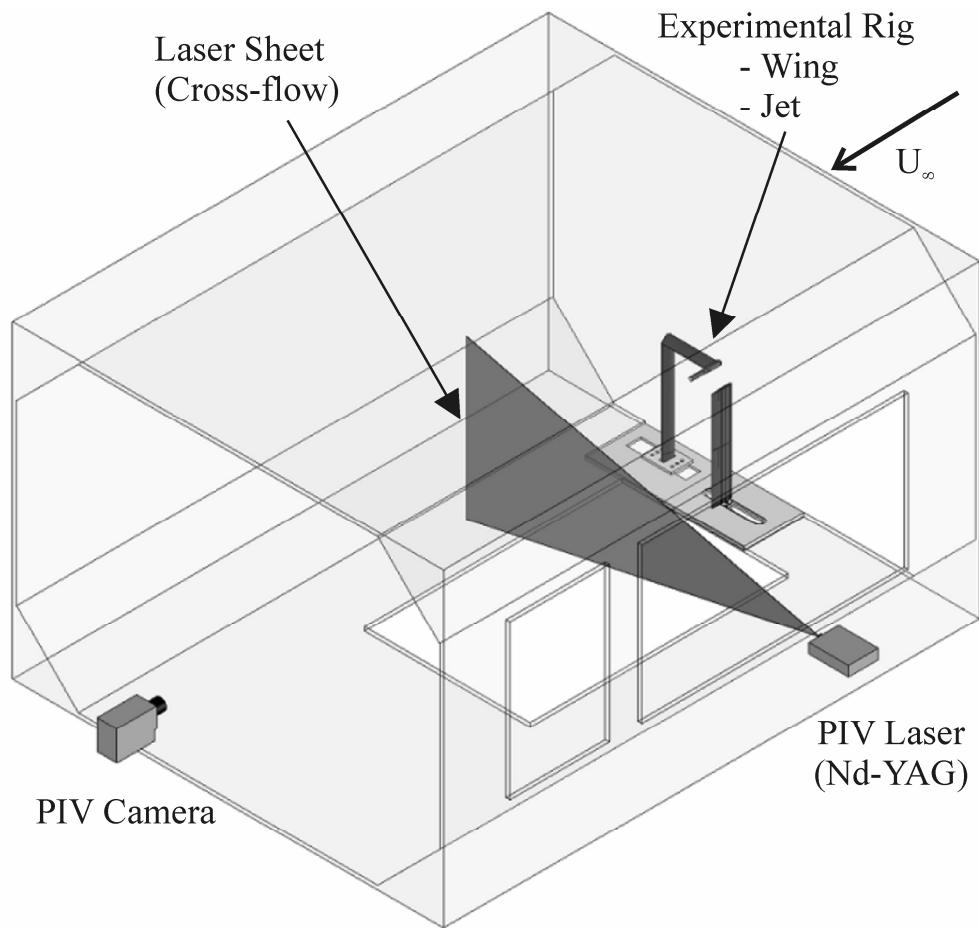


Figure 2. Experimental setup in the 7' x 5' (large) wind tunnel.

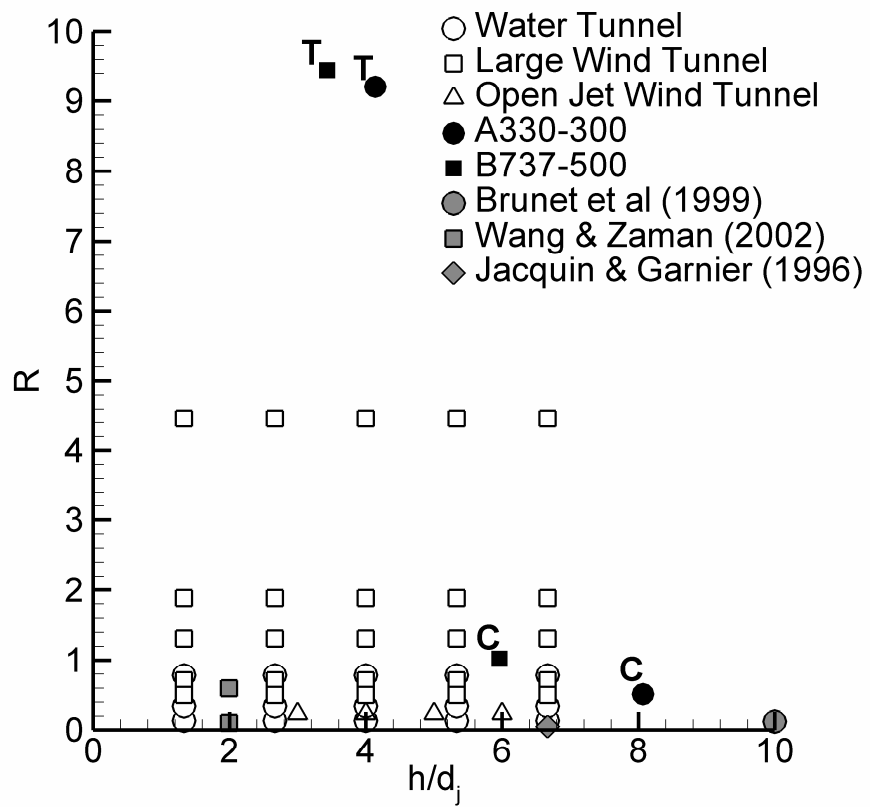


Figure 3. The main parameter space examined.

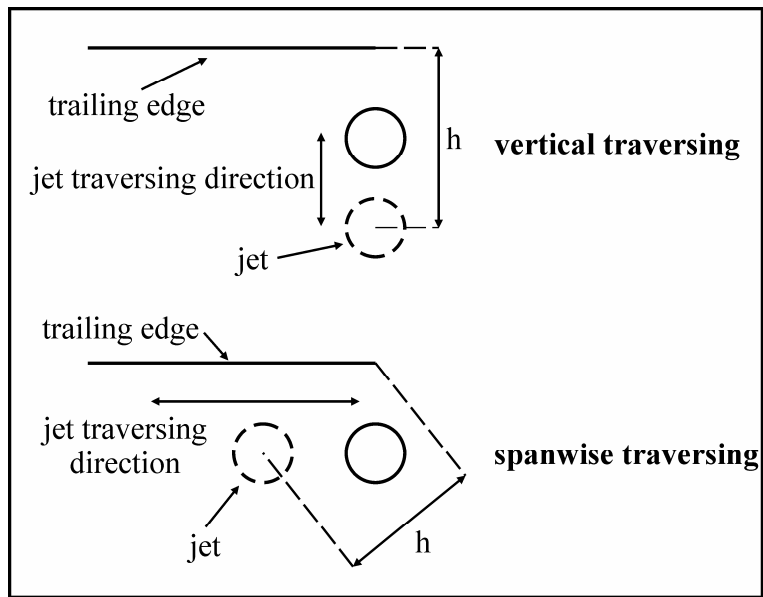


Figure 4. Definition of the two traversing directions and of the jet-to-tip distance (h) parameter.

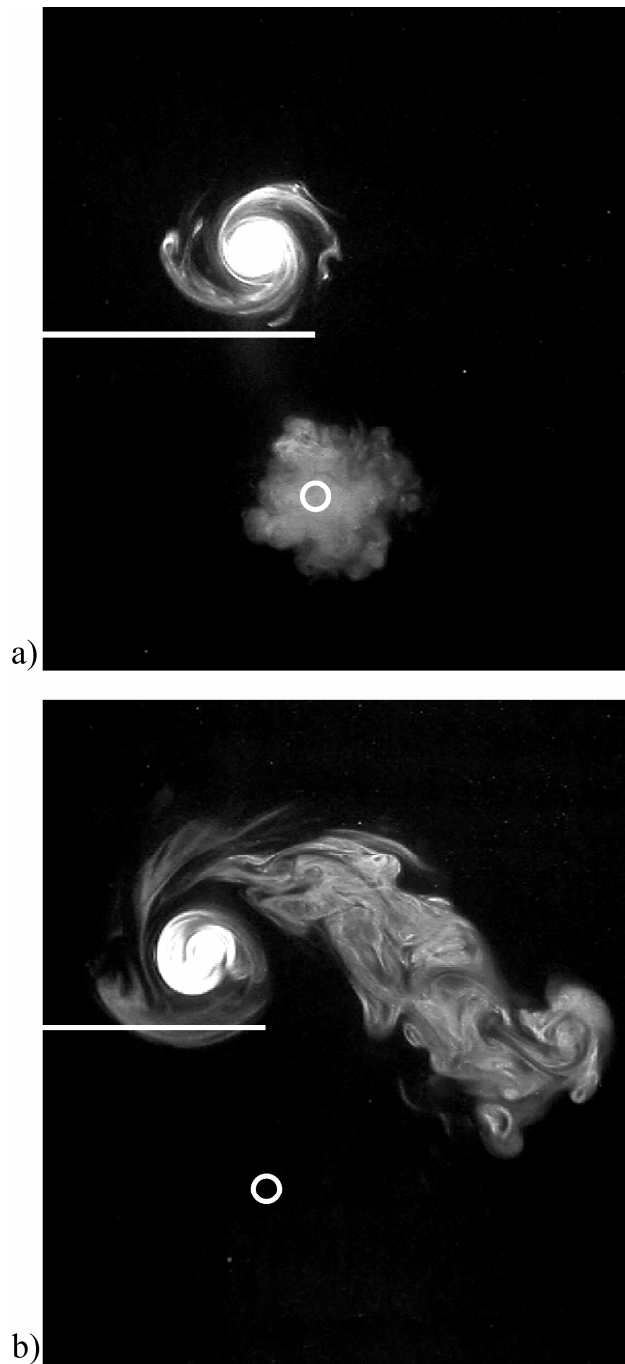


Figure 5. Instantaneous flow visualization images (water tunnel) for $Re_\Gamma = 5500$, $h/d_j = 6.7$, $U_j/U_\infty = 2.01$, $R = 0.13$, a) $x/b = 0.35$ ($x/d_j = 26.7$), b) $x/b = 1.75$ ($x/d_j = 133.3$).

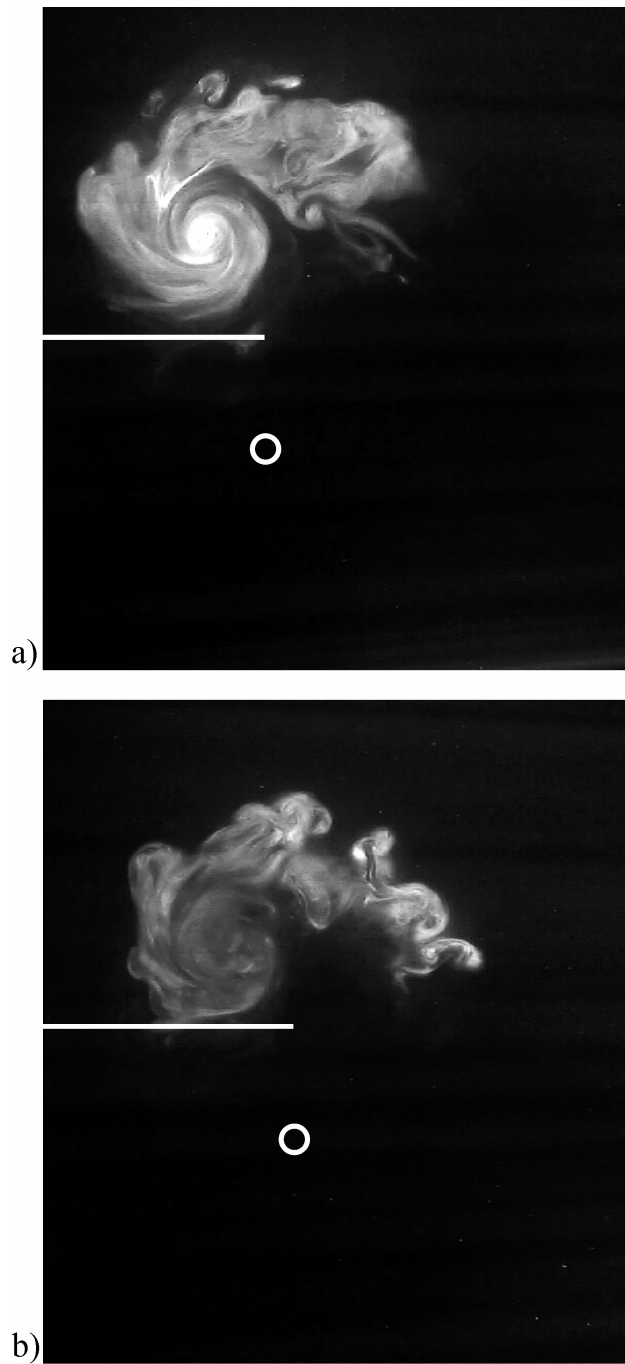


Figure 6. Instantaneous flow visualization images (water tunnel) for $Re_\Gamma = 5500$, $h/d_j = 4$, $U_j/U_\infty = 2.01$, $R = 0.13$, $x/b = 1.75$ ($x/d_j = 133.3$). a) Both jet and vortex visualized, b) only jet visualized.

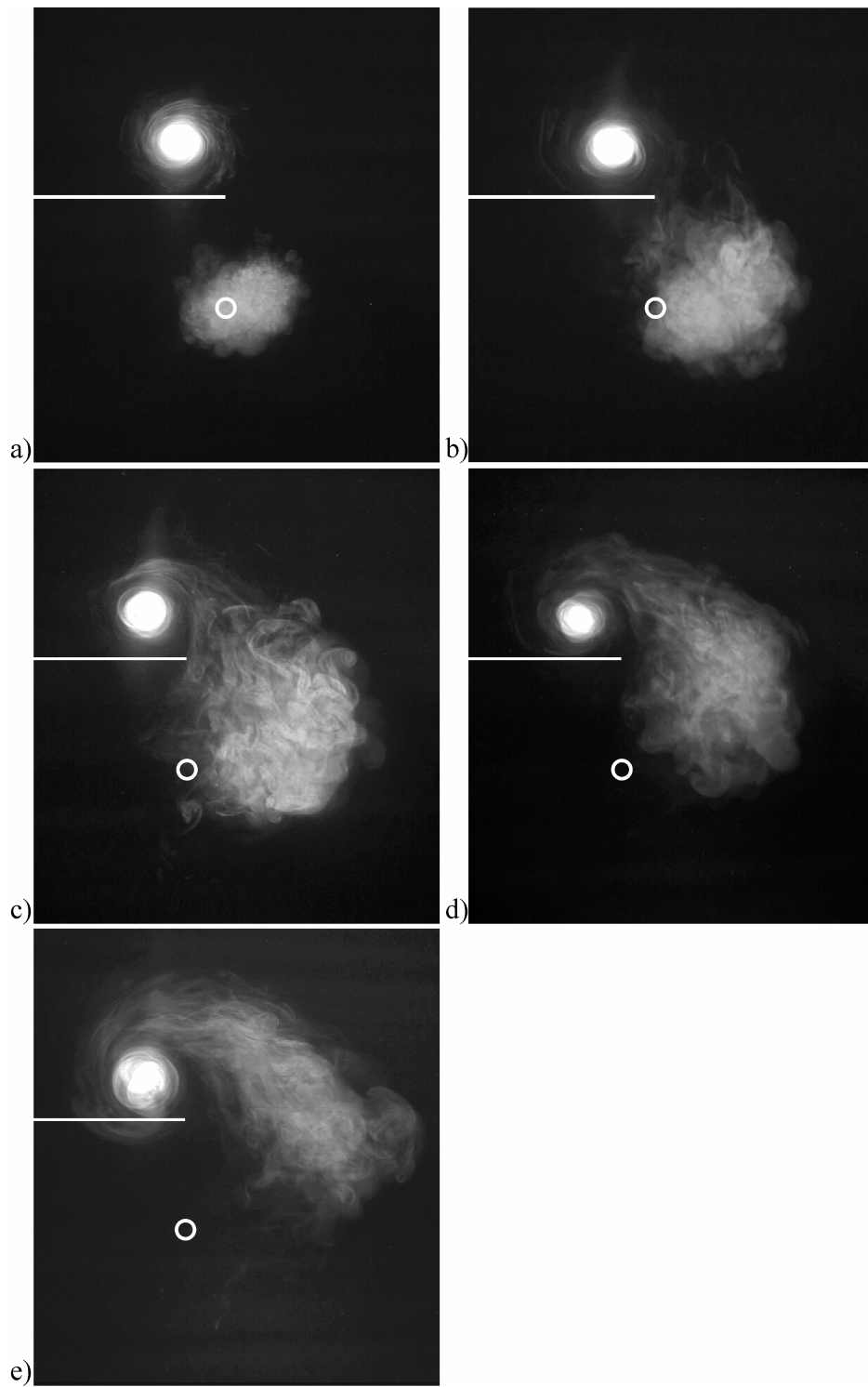


Figure 7. Time-averaged flow visualization images (water tunnel). Streamwise development for $Re_T = 5500$, $h/d_j = 6.7$, $U_j/U_\infty = 2.01$, $R = 0.13$. a) $x/b = 0.35$ ($x/d_j = 26.7$), b) $x/b = 0.7$ ($x/d_j = 53.3$), c) $x/b = 1.05$ ($x/d_j = 80$), d) $x/b = 1.4$ ($x/d_j = 106.7$), e) $x/b = 1.75$ ($x/d_j = 133.3$).

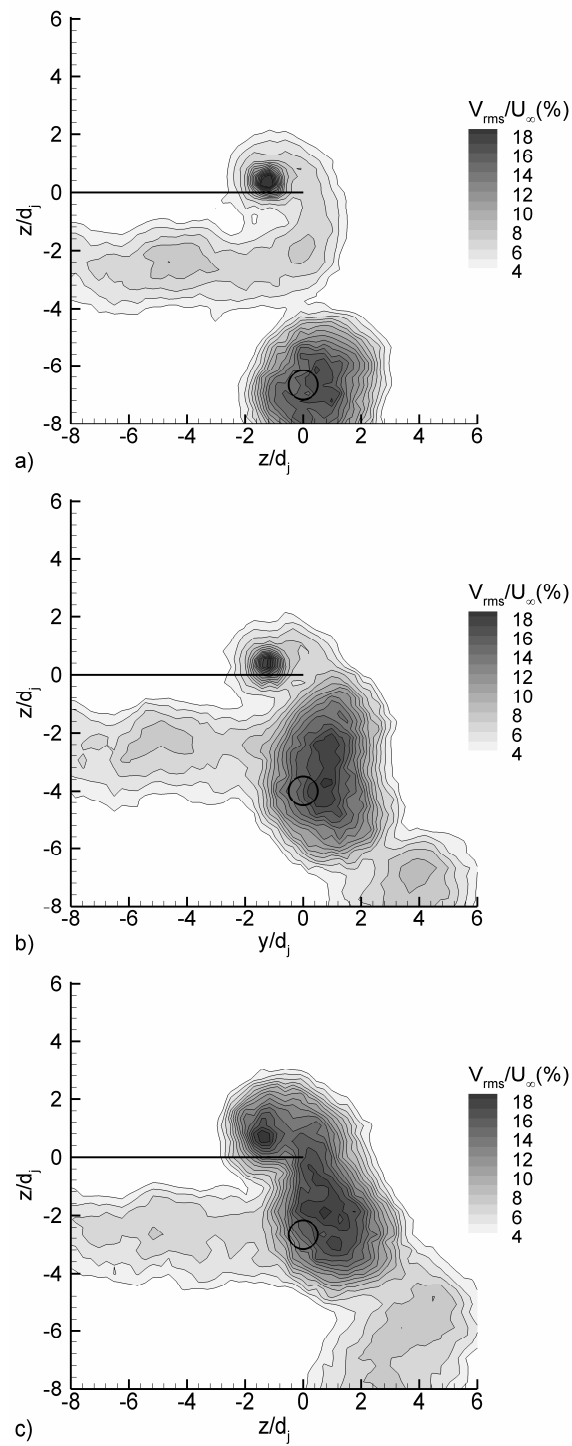


Figure 8. Standard deviation of the cross-flow velocity (water tunnel experiments) for $Re_{\Gamma} = 5500$, $U_j/U_{\infty} = 2.85$, $R = 0.34$, $x/b = 0.35$ ($x/d_j = 26.7$), a) $h/d_j = 6.7$, b) $h/d_j = 4$, c) $h/d_j = 2.7$.

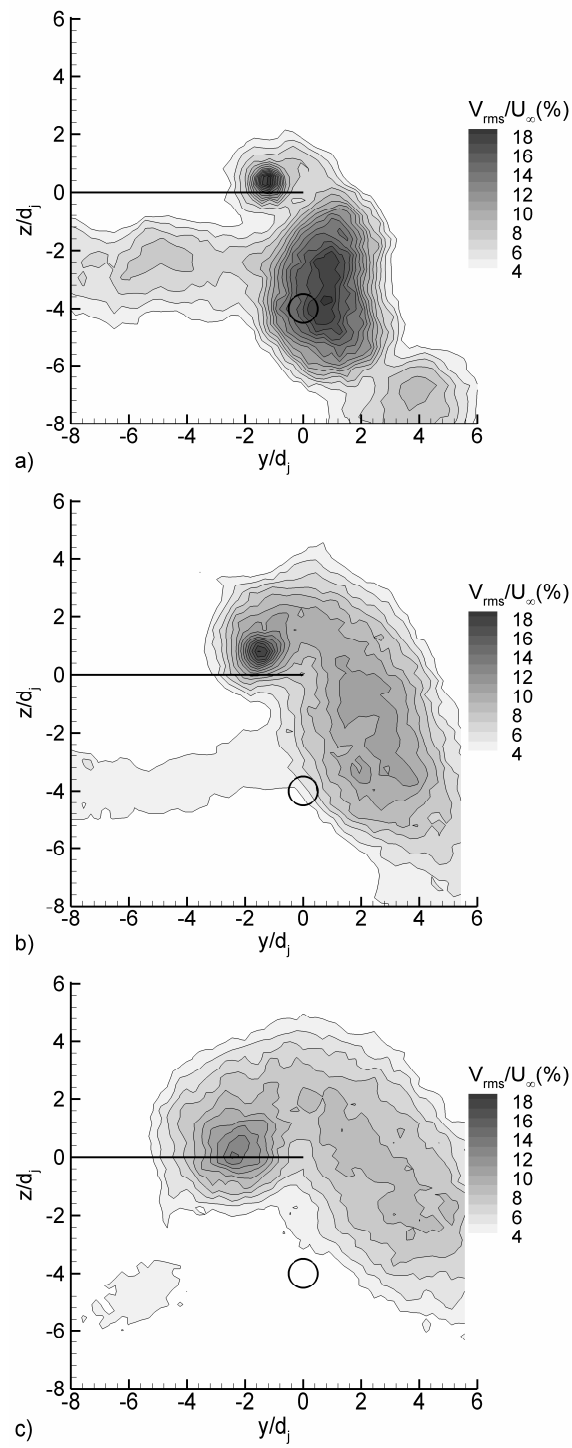


Figure 9. Standard deviation of the cross-flow velocity (water tunnel experiments) for $Re_{\Gamma} = 5500$, $U_j/U_{\infty} = 2.85$, $R = 0.34$, $h/d_j = 4$, a) $x/b = 0.35$ ($x/d_j = 26.7$), b) $x/b = 0.7$ ($x/d_j = 53.3$), c) $x/b = 1.05$ ($x/d_j = 80$).

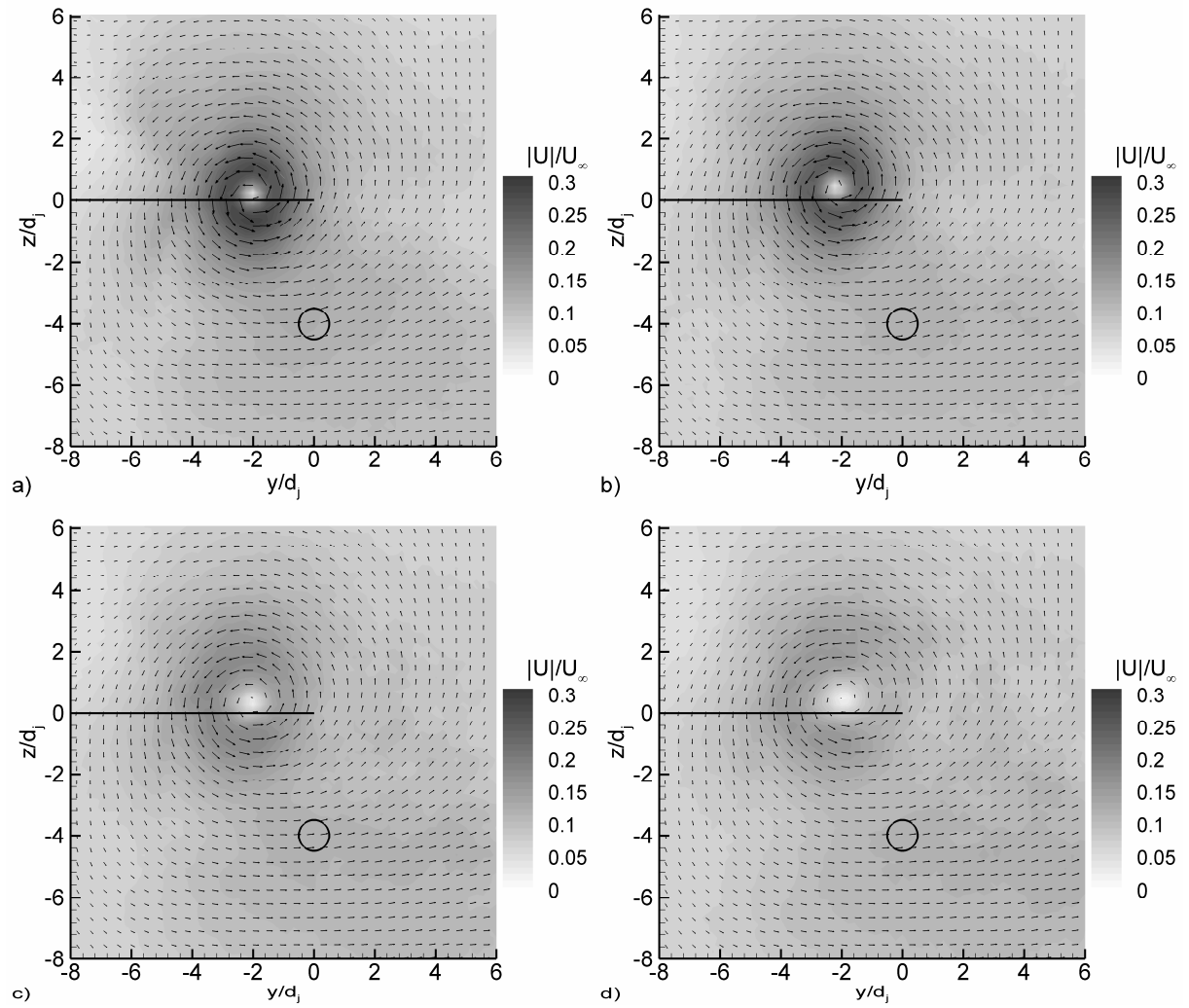


Figure 10. Time-averaged cross-flow velocity magnitude (water tunnel experiments) for $Re_T = 5500$, $h/d_j = 4$, $x/b = 1.05$ ($x/d_j = 80$), a) $U_j/U_\infty = 0$, b) $U_j/U_\infty = 2.01$, $R = 0.13$, c) $U_j/U_\infty = 2.85$, $R = 0.34$, d) $U_j/U_\infty = 4.03$, $R = 0.78$. Every second vector is plotted.

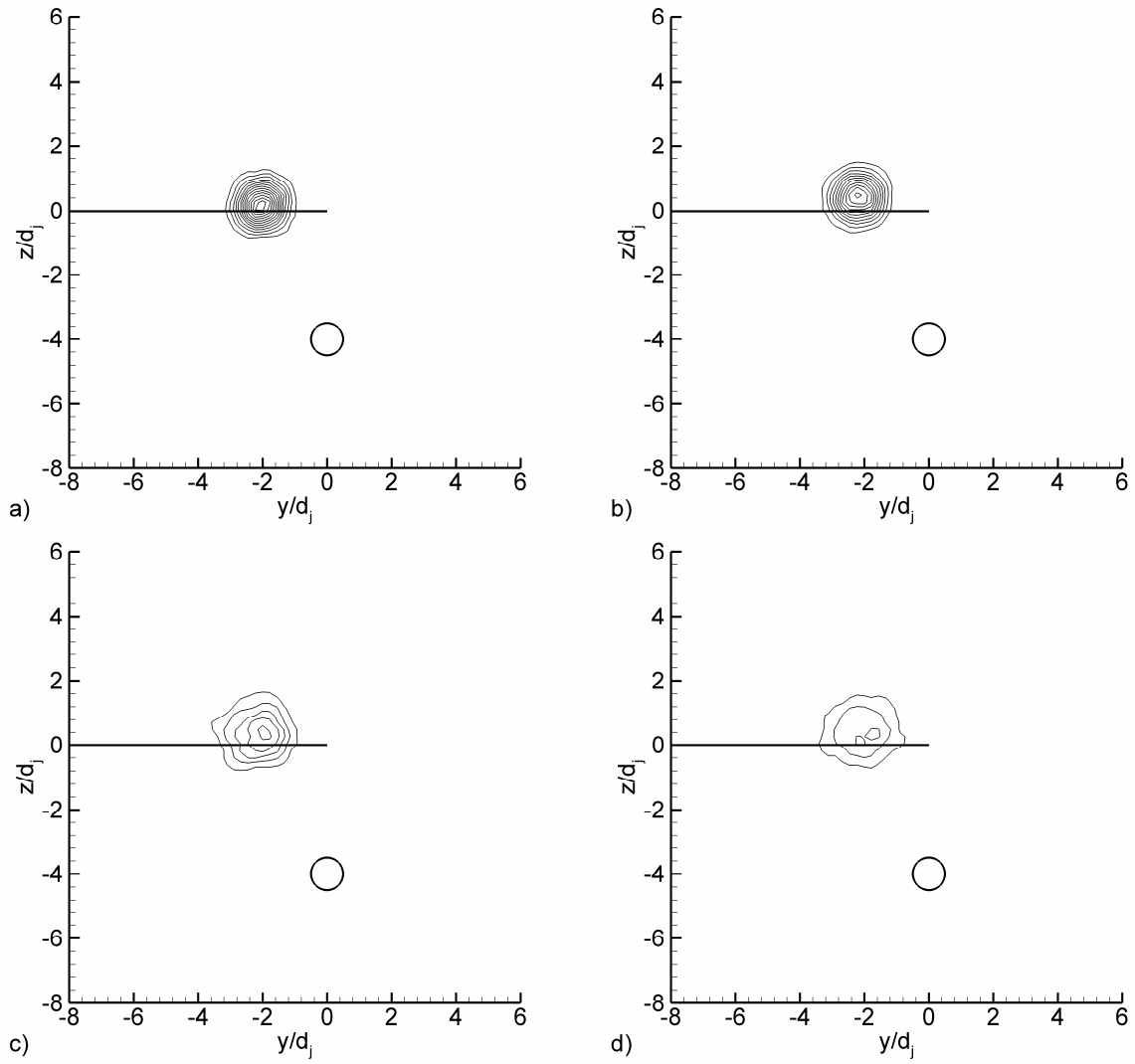


Figure 11. Time-averaged vorticity normalized by chord length and free stream velocity, (water tunnel experiments) for $Re_T = 5500$, $h/d_j = 4$, $x/b = 1.05$ ($x/d_j = 80$), a) $U_j/U_\infty = 0$, b) $U_j/U_\infty = 2.01$, $R = 0.13$, c) $U_j/U_\infty = 2.85$, $R = 0.34$, d) $U_j/U_\infty = 4.03$, $R = 0.78$. Minimum contour level $\omega c/U_\infty = 1$, increment 0.5.

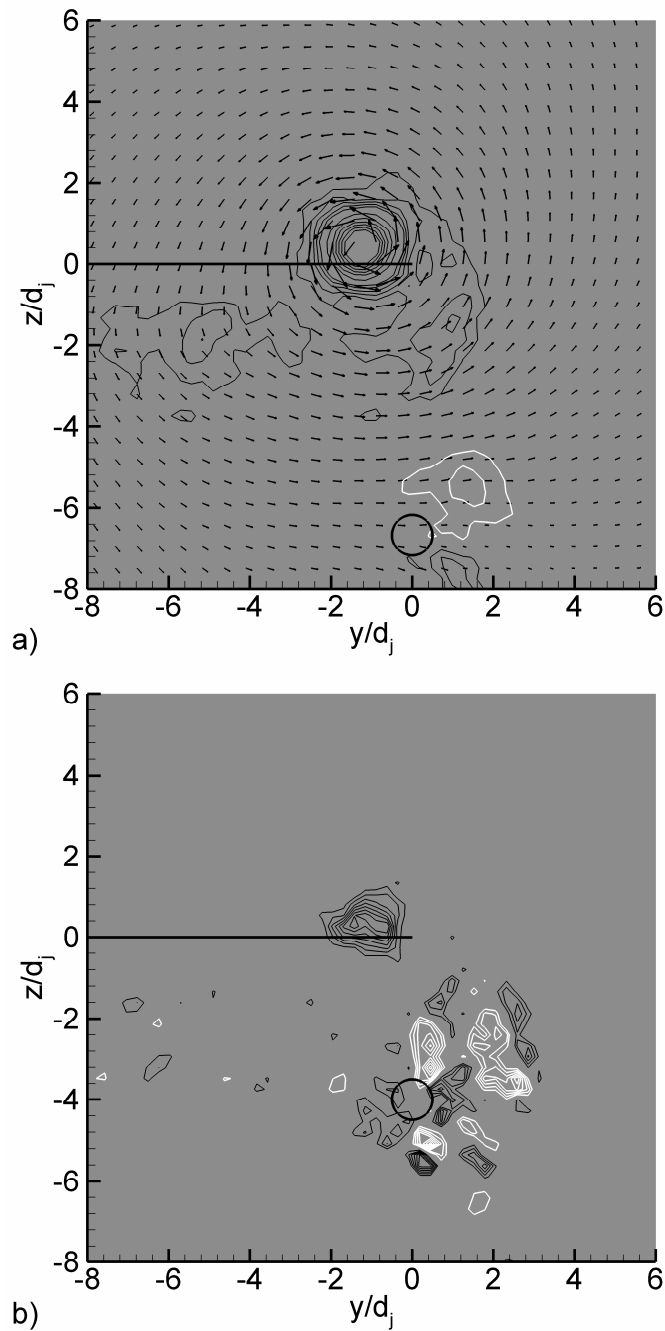


Figure 12. Vorticity normalized by chord length and free stream velocity, (water tunnel experiments) for $Re_T = 5500$ and $x/b = 0.35$ ($x/d_j = 26.7$). Black lines: positive values; white lines: negative values. a) Time-averaged field, $h/d_j = 6.7$, $U_j/U_\infty = 2.01$, $R = 0.13$. Minimum contour level $|\omega c/U_\infty| = 0.2$, increment 0.2 until $|\omega c/U_\infty| = 1$ and then increment 1. Every second velocity vector is plotted. b) Instantaneous field, $h/d_j = 4$, $U_j/U_\infty = 4.03$, $R = 0.78$. Minimum contour level $|\omega c/U_\infty| = 2$, increment 1.

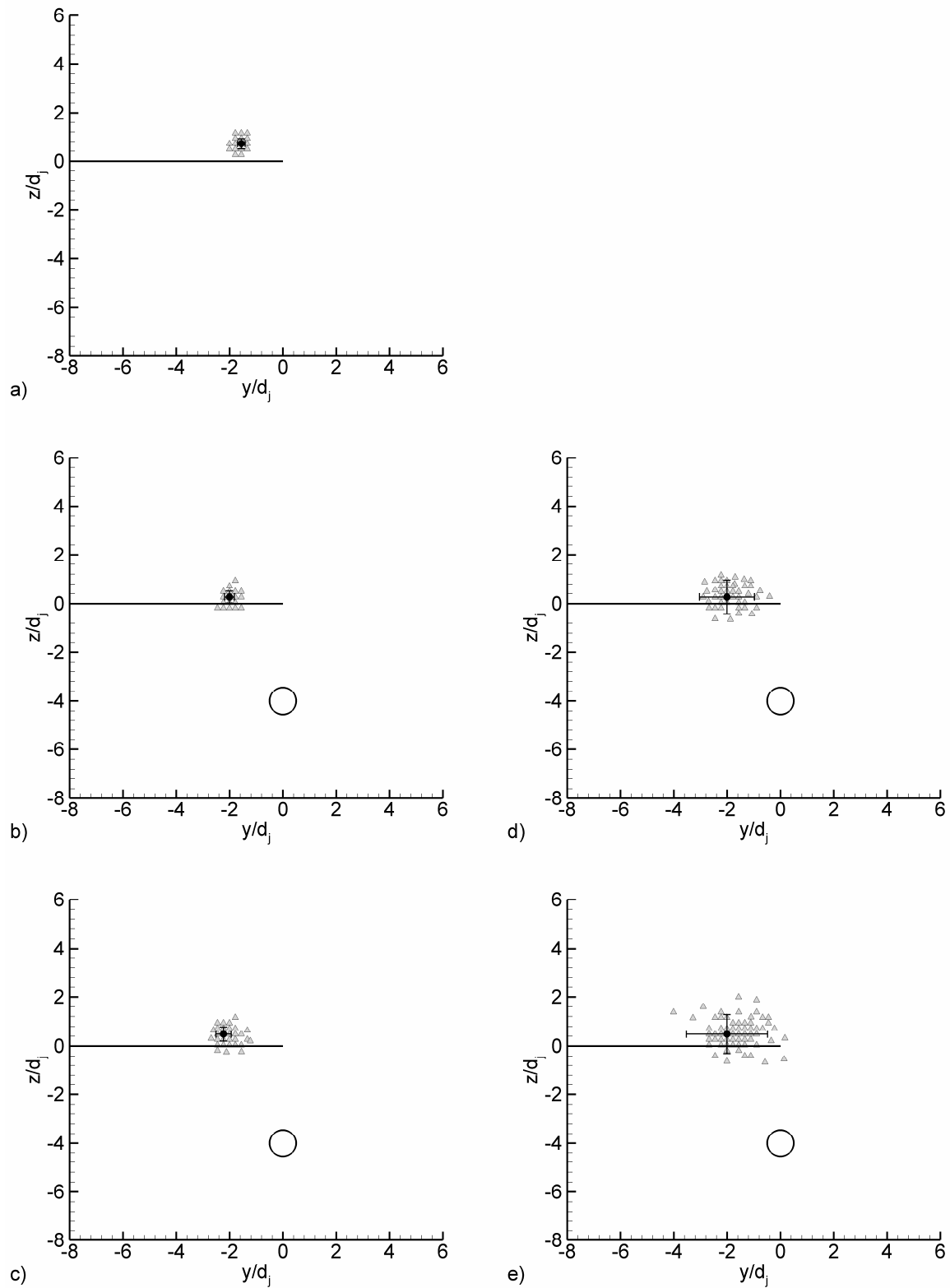


Figure 13. Vortex center position (water tunnel experiments) for $Re_\Gamma = 5500$, $h/d_j = 4$, $x/b = 1.05$ ($x/d_j = 80$). a) reference case, b) $U_j/U_\infty = 0$, c) $U_j/U_\infty = 2.01$, $R = 0.13$, d) $U_j/U_\infty = 2.85$, $R = 0.34$, e) $U_j/U_\infty = 4.03$, $R = 0.78$. The gray symbols show the instantaneous whereas the black symbols the time-averaged vortex center. The error bars indicate the standard deviation in each direction.

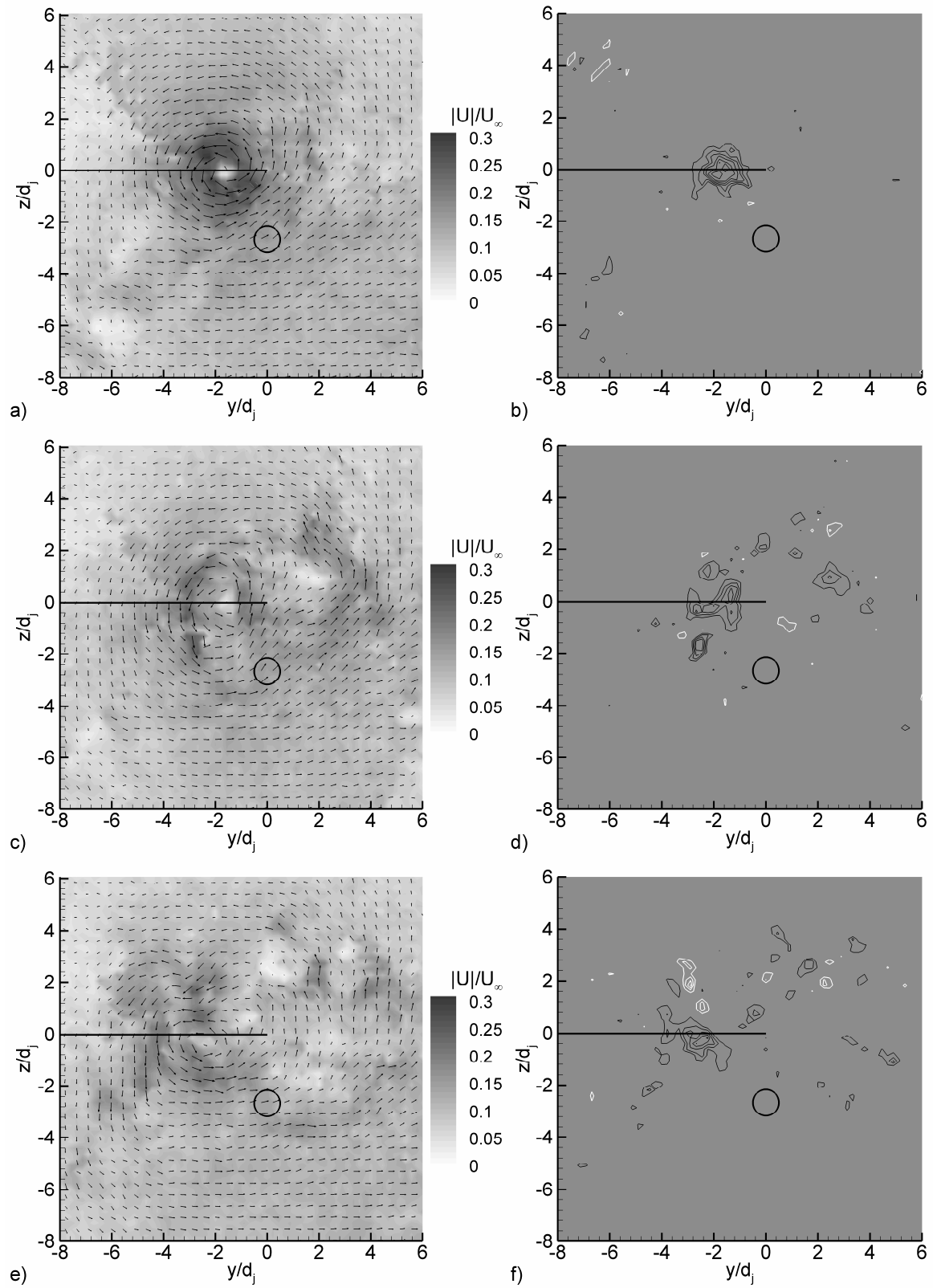


Figure 14. Instantaneous cross-flow velocity magnitude and normalized vorticity (water tunnel experiments) for $Re_{\Gamma} = 5500$, $h/d_j = 2.7$, $x/b = 1.05$ ($x/d_j = 80$), a)-b) $U_j/U_{\infty} = 0$, c)-f) $U_j/U_{\infty} = 2.85$, $R = 0.34$. Every second velocity vector is plotted. Vorticity contours: black lines: positive values; white lines: negative values; minimum level $|\omega c/U_{\infty}| = 1.5$, increment 1.

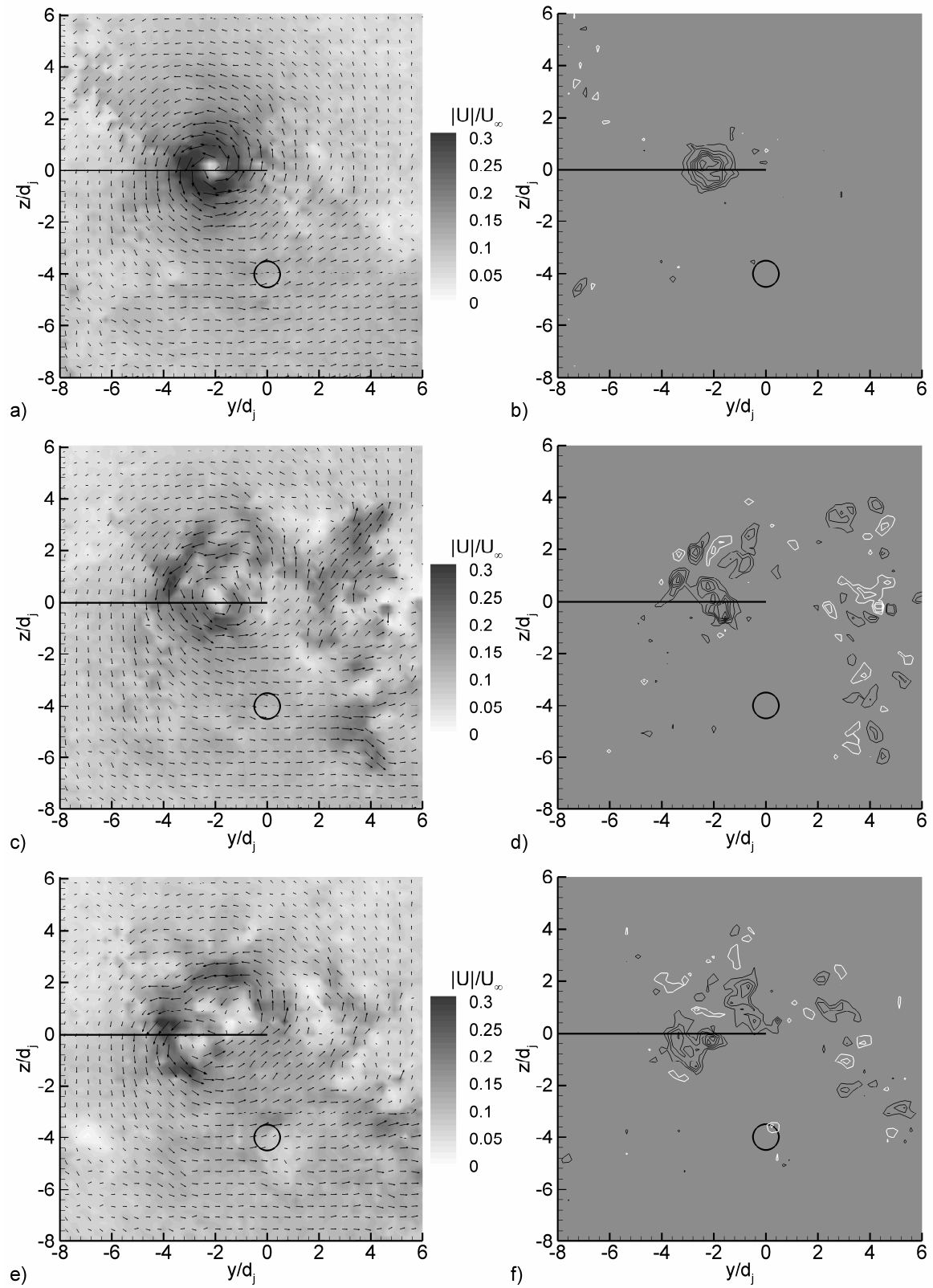


Figure 15. Instantaneous cross-flow velocity magnitude and normalized vorticity (water tunnel experiments) for $Re_\Gamma = 5500$, $h/d_j = 4$, $x/b = 1.05$ ($x/d_j = 80$), a)-b) $U_j/U_\infty = 0$, c)-f) $U_j/U_\infty = 2.85$, $R = 0.34$. Every second velocity vector is plotted. Vorticity contours: black lines: positive values; white lines: negative values; minimum level $|\omega c/U_\infty| = 1.5$, increment 1.

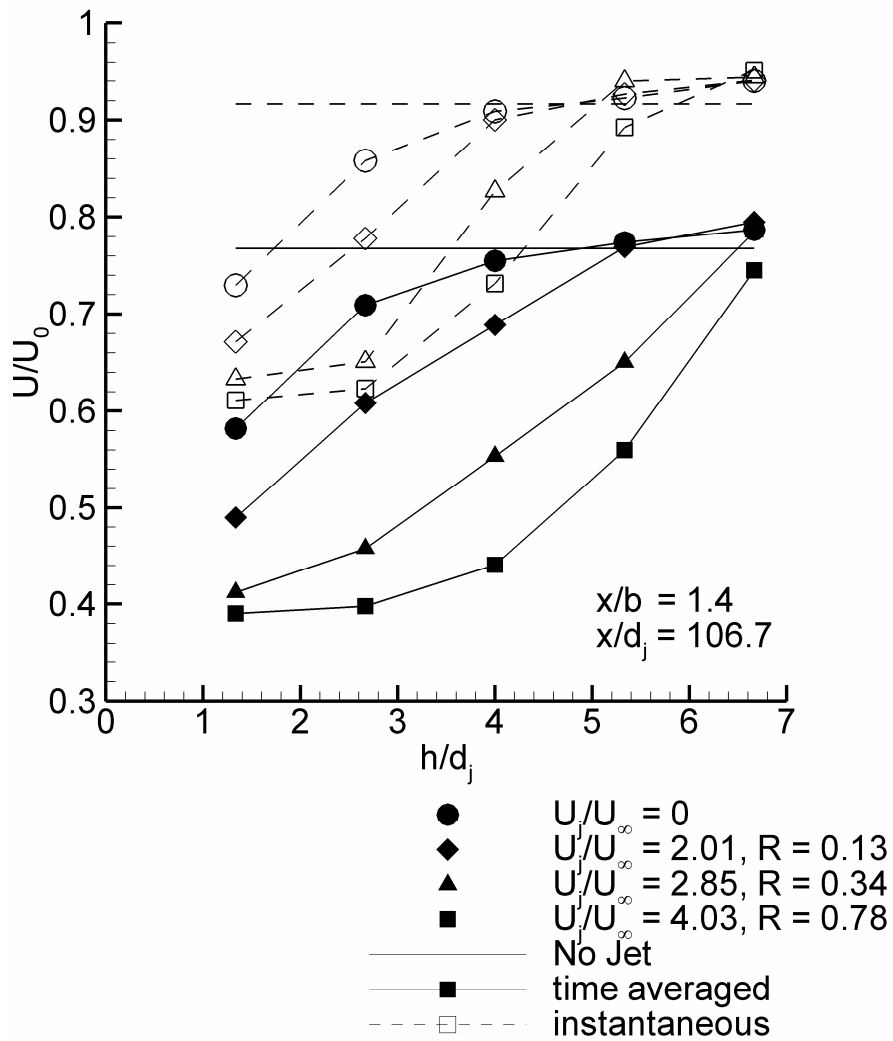


Figure 16. Time-averaged and mean instantaneous value of the maximum cross-flow velocity magnitude around the vortex core as a function of jet-to-tip distance and R (water tunnel experiments) for $Re_T = 5500$, $x/b = 1.4$ ($x/d_j = 106.7$).

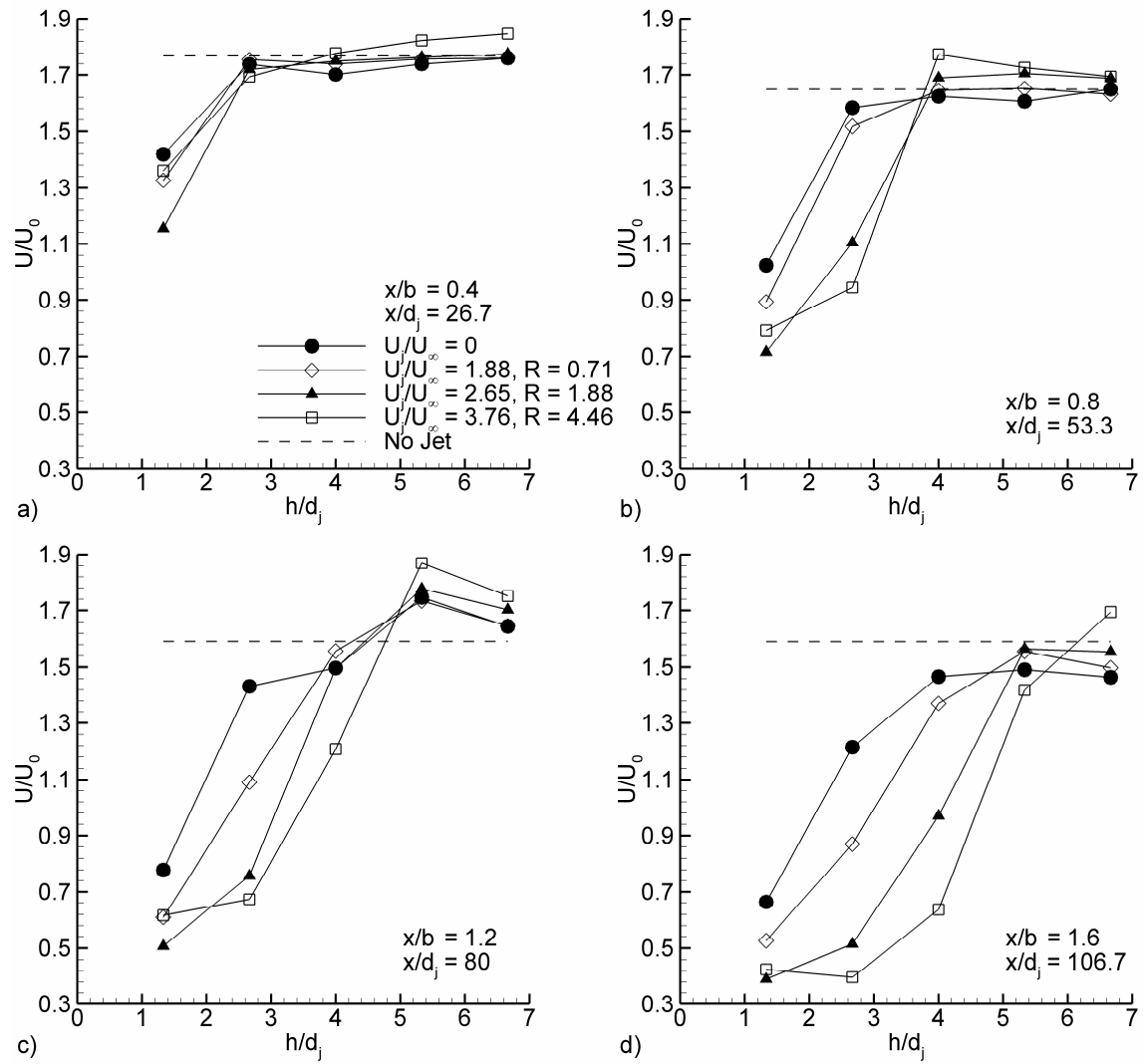


Figure 17. Mean value of the instantaneous maximum cross-flow velocity magnitude around the vortex core as a function of jet-to-tip distance and R (large wind tunnel experiments) for $Re_\Gamma = 14000$, a) $x/b = 0.4$ ($x/d_j = 26.7$), b) $x/b = 0.8$ ($x/d_j = 53.3$), c) $x/b = 1.2$ ($x/d_j = 80$), d) $x/b = 1.6$ ($x/d_j = 106.7$).

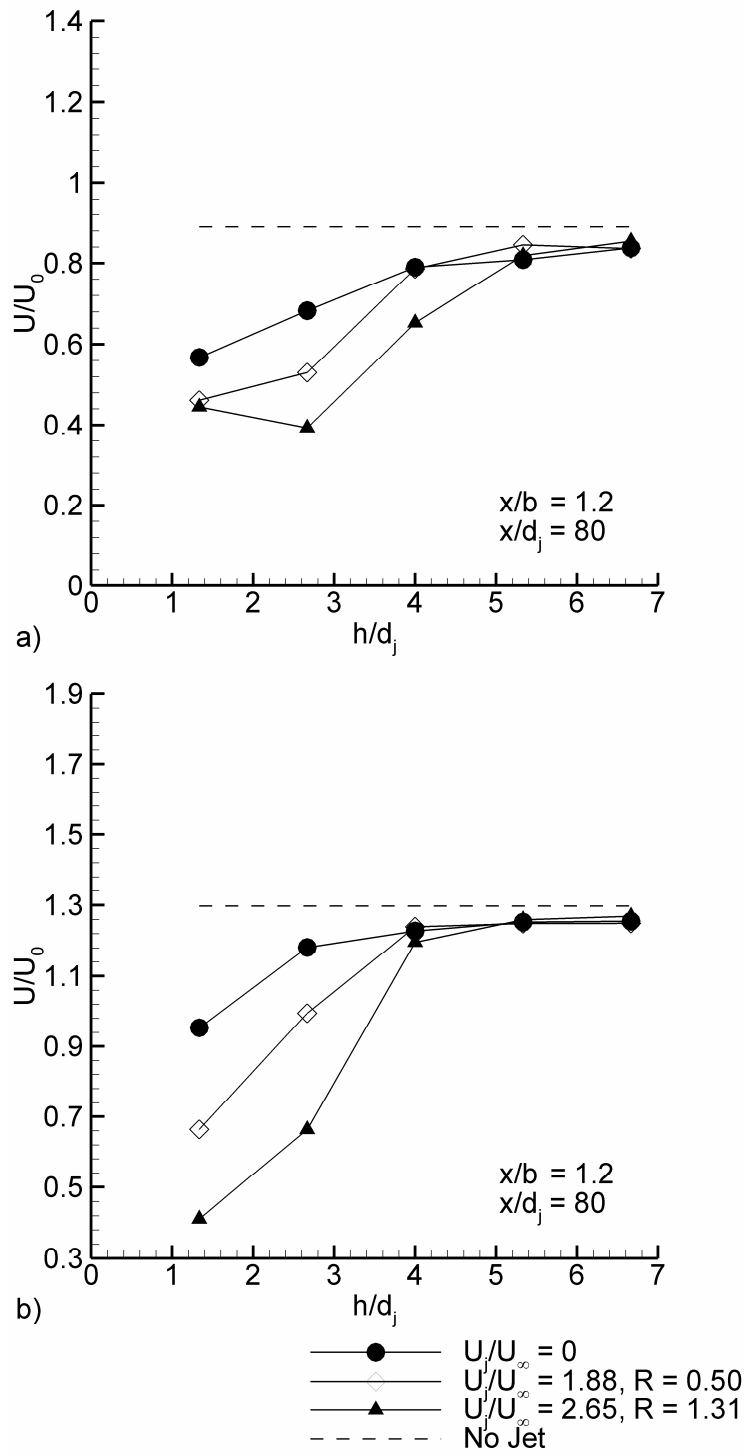


Figure 18. Analysis results for the high Reynolds number ($Re_T = 33000$) experiments (large wind tunnel experiments). All parameters shown as a function of jet-to-tip distance and R . a) time-averaged maximum cross-flow velocity magnitude around the vortex core, b) mean value of the instantaneous maximum cross-flow velocity magnitude around the vortex core.

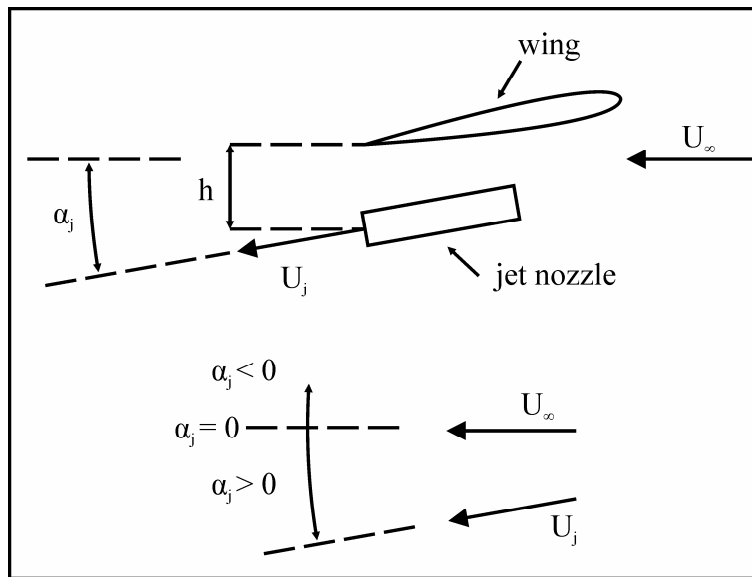


Figure 19. Definition of the angle between the jet exit velocity and the free stream (jet angle).

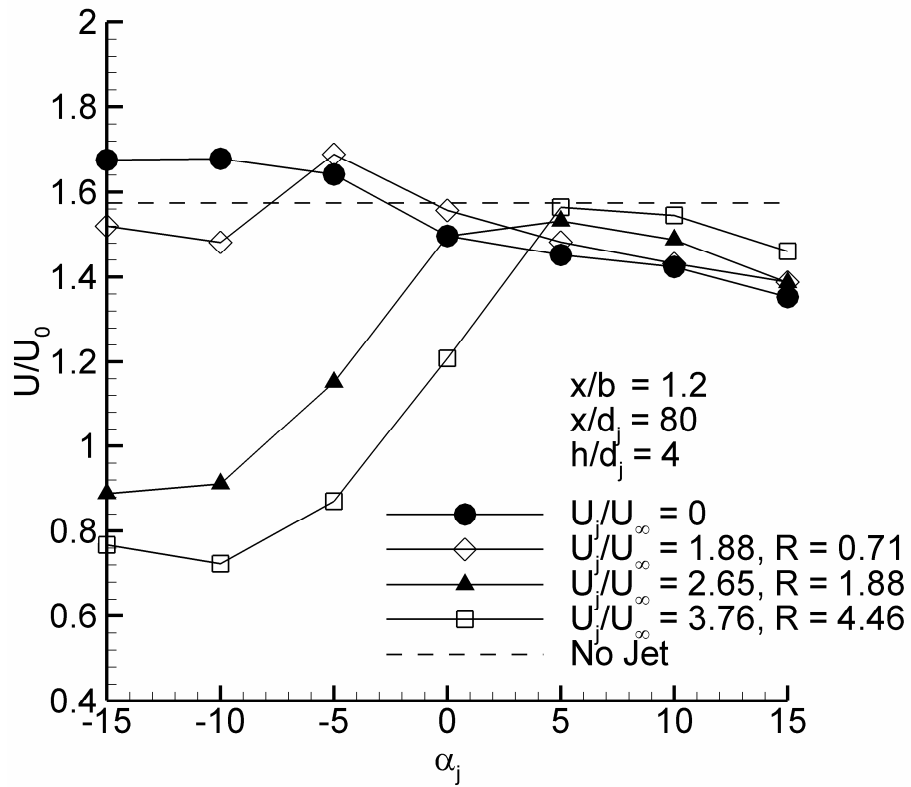


Figure 20. Mean value of the instantaneous maximum cross-flow velocity magnitude around the vortex core as a function of the jet angle and R (large wind tunnel experiments) for $Re_\Gamma = 14000$, $x/b = 1.2$ ($x/d_j = 80$).